CONF-8706112--1

CONF-8706112--1

DE87 010377

THE EMITTANCE AND BRIGHTNESS CHARACTERISTICS OF NEGATIVE ION SOURCES SUITABLE FOR MeV ION IMPLANTATION*

G. D. Alton
Physics Division
Oak Ridge National Laboratory
Post Office Box X
Oak Ridge, Tennessee 37831 USA

1. Introduction

High-energy ion implantation (at energies between 0.5 and 10 MeV) into semiconducting materials is being used at an increasing rate for preparation of active regions between buried layers and to provide isolation barriers in devices. Increasingly higher energies are required because of device fabrication with deeper active layers. Attempts to use high-energy implantation in practical applications dates back to the 1960s with emphasis on its usage in material modifications, recoil damaging, amorphization, annealing, solid-state epitaxy, particle detectors, and reduction of minority carrier lifetimes, etc. Commercial markets for most of these techniques were very limited because of readily available and less expensive alternatives. However, in recent years, the revival of CMOS technology and the need for latch-up and single-event immunity have created a need for deep layer isolation barriers beneath active regions of a particular device. To date, one of the most promising approaches to substrate isolation is separation by implantation of oxygen (SIMOX), which also has the beneficial effects of lower leakage currents and faster switching speeds for devices. High-energy implantation is also being used for the creation of CMOS p-wells which utilize much lower power and offer greater latch-up immunity. The number of other applications for high-energy ion implantation continues to grow, such as the programming of read-only memory chips (ROMs), grid formation for charge collection in dynamic random access memory chips (RAMS), junction field emission transistors (FETs), ion lithography, mask replication, and wave guide formation. For additional information on the subject of ion implantation applications, the reader is referred to review articles such as [1] and to the proceedings of recent ion implantation conferences [2].

The dose levels required for many of these applications range from 10^{15} to 10^{18} atoms/cm^2. Achievement of such high dose levels in reasonable times places a premium on the performance characteristics (emittance and brightness) of the ion source utilized in the ion implantation process. While the future trends may emphasize the utilization of high-current, linac-type accelerators now under active development [3] and, consequently, the use of high-intensity positive ion sources with several mA of ion current capabilities, considerable efforts have been devoted by commercial firms in developing small, relatively high-current MeV ion implantation systems based on the tandem electrostatic accelerator principle [4,5] and the consequent use of negative ion sources for the generation of ion beams for such applications. This paper provides the description and beam properties of ion sources suitable for use with such devices. Particular emphasis is placed on the emittance and brightness properties of state-of-the-art, high-intensity, negative ion sources based on the cesium ion sputter principle. Because of the high efficiency of the charge

*Research sponsored by the Division of Basic Energy Sciences, U.S. Department of Energy, under contract DE-AC05-84OR21400 with Martin Marietta Energy Systems, Inc.

"The submitted manuscript has been authored by a contractor of the U.S. Government under contract No. DE-AC05-84OR21400. Accordingly, the U.S. Government retains a nonexclusive, royalty-free license to publish or reproduce the published form of this contribution, or allow others to do so, for U.S. Government purposes."

DISCLAIMER

This report was prepared as an account of work sponsored by an agency of the United States Government. Neither the United States Government nor any agency thereof, nor any of their employees, makes any warranty, express or implied, or assumes any legal liability or responsibility for the accuracy, completeness, or usefulness of any information, apparatus, product, or process disclosed, or represents that its use would not infringe privately owned rights. Reference herein to any specific commercial product, process, or service by trade name, trademark, manufacturer, or otherwise does not necessarily constitute or imply its endorsement, recommendation, or favoring by the United States Government or any agency thereof. The views and opinions of authors expressed herein do not necessarily state or reflect those of the United States Government or any agency thereof.

MASTER

34A

DISTRIBUTION OF THIS DOCUMENT IS UNLIMITED

exchange mechanism for negative ion generation, renewed efforts are under way to utilize this technique for increasing the negative ion beam intensities over other available techniques [6].

2. Definitions

Perhaps the most important attribute of an ion beam is that it have properties compatible with the beam transport system that it must pass through. The quality of an ion beam in this regard is usually expressed in terms of the emittance ϵ and brightness B. Both are related through the ion current I and are direct consequences of Liouville's theorem. The acceptance A for a beam transport system is the complement of the emittance ϵ and thus must be greater than ϵ to ensure beam transport through the system.

2.1. Liouville's Theorem

This fundamental theorem postulates that the motion of a group of particles under the action of conservative force fields is such that the local number density in the six-dimensional phase space (x,y,z,Px,Py,Pz) (hypervolume) everywhere remains constant. An ion beam can be represented by a group of points, all of which lie within the six-dimensional hypervolume. The phase space volume of an ion beam may increase due to interactions with residual gas particles and/or gas and foil strippers, beam transport and acceleration system aberrations, and space charge effects, but can never be less than its value immediately following extraction from the source. Thus, the magnitude of the phase space volume or quantity proportional to the phase space volume (emittance) measured immediately following extraction is a unique characteristic of the particular ion source.

2.2. Emittance

If the transverse components of motion of a group of particles are mutually independent in configuration space (i.e., neglecting space charge and spin-dependent interactions), the motion of the particles in the orthogonal planes (x,Px), (y,Py), and (z,Pz) will be uncoupled and, therefore, can be treated separately. For uncoupled motion in which a beam is moving along the z direction under the action of conservative forces, the four-dimensional hyperarea (x,Px,y,Py) or transverse phase space, is a conserved quantity according to Liouville's theorem.

For the case where Pz is constant, the transverse momenta Px,Py can be replaced by corresponding angular components, since

$$\frac{Px}{Pz} = \tan \theta x \cong \frac{dx}{dz} = x' \qquad (1)$$

and

$$\frac{Py}{Pz} = \tan \theta y \cong \frac{dy}{dz} = y' \qquad (2)$$

in the small-angle approximation. The respective transverse phase space areas then are proportional to the areas (x,x') and (y,y').

To account for changes in the axial momentum Pz of an ion beam, the concept of normalized emittance is often used. We define the orthogonal normalized emittances as

$$\epsilon_{nx} = \pi x x' \sqrt{E} \qquad (3)$$

and

$$\varepsilon_{ny} = \pi y y' \sqrt{E}, \quad (4)$$

where E is the energy of the ion beam. The units of emittance are often given in terms of π mm mrad $(MeV)^{1/2}$.

We define the two-dimensional normalized emittance as the square root of the product of the normalized emittances associated with the (x,x') and (y,y') areas, or $\varepsilon_n = (\varepsilon_{nx}\varepsilon_{ny})^{1/2}$.

2.3. Brightness

Another figure of merit often used for evaluating the quality of ion beams is the brightness B. Brightness is defined in terms of the ion current dI per unit area dS per unit solid angle dΩ or

$$B = \frac{dI}{dS d\Omega} \cdot \quad (5)$$

According to Walsh [7], brightness can be related to the normalized emittance of the ion beam through the following expression:

$$B = \frac{2I}{\varepsilon_{nx}\varepsilon_{ny}} = \frac{2I}{(\varepsilon_n)^2} \cdot \quad (6)$$

3. Emittance Measurement Facility

Emittance measurements of the ion beams extracted from the sources utilized in these investigations were determined by use of the equipment and procedures described in the following parts of this section. The sources were mounted on a test stand equipped with capabilities for accelerating negative ion beams up to energies of 30 keV with energies of 20 keV typical of all measurements [8]. The facility consists of a negative ion source, a conventional three-cylinder einzel lens, a double-focusing magnet, the emittance measuring device, beam line component valves, turbomolecular pumping stations, and auxiliary power supplies required for system operation. Negative ion beams are extracted from the source and focused by means of the einzel lens onto the object plane of the magnet. Ions of the desired mass are then deflected through 90° and focused at the image position of the system. The intensity of the negative ion beam can be monitored prior to and following momentum analysis by insertion of remotely actuatable Faraday cups; the Faraday cups are located immediately behind variable slit-type apertures which are positioned at the object and image planes of the momentum analysis system. With the Faraday cups removed, the beam can be focused downstream onto the slit detector unit of the emittance measurement device and determinations made of the emittances and brightnesses of dc or pulsed negative ion beams. Emittance measurements can be effected automatically through the use of the microcomputer CAMAC-based data acquisition and hardware control system described previously [8,9].

3.1. The Emittance Measuring Apparatus

The emittance measurement device consists of a vacuum housing, two identical stepping motor-driven detector units for determining the emittances of an ion beam in either the x or y directions, and a control unit for driving the detector hardware. The control unit consists of a microcomputer which is interfaced to a CAMAC crate controller, an input/output register, a stepping motor controller, and a 12-bit analog-to-digital converter (ADC). The CAMAC crate control modules communicate with the emittance measurement hardware via

an external electronics unit.

The ion beam dignostic unit, shown in Fig. 1, consists of an electrically isolated slit aperture, positioned 0.4 m in front of a detector unit which is made up of 32 electrically isolated plates. The current striking each of the detectors is used to determine the differential angular divergence of the ion beamlet which is allowed to pass through the slit aperture at a given x or y position. An emittance measurement consists of stepping the slit detector system through an ion beam in a chosen direction while monitoring the total ion current striking the slit unit and the differential ion currents striking each of the 32 detectors during a selectable integration time period. The signals are integrated, digitized, and stored in memory of the microcomputer for later data analysis.

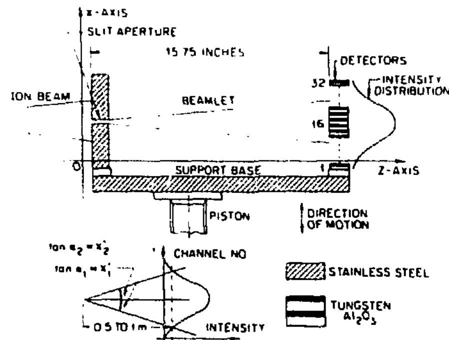

Fig. 1. Schematic drawing of the emittance measurement detector unit.

4. Negative Ion Source Descriptions

The technology for producing high intensity negative ion beams with improved beam qualities from sources based on the sputter principle [10] has advanced significantly during the past few years. A number of single-aperture sputter-type sources have been reported in the literature [11-17]. In such sources, the sample material is mounted on a negatively biased probe which is maintained at a potential difference with respect to the housing of 1-5 kV negative in a controlled flux of a neutral Group IA element, usually cesium, which effects a lowering of the work function [18] and enhances the probability for negative ion formation during the sputter ejection process [19]. Sputtering of the sample material is effected by bombardment with positive Group IA element ions which are formed by direct surface ionization during collisions with a hot, high work function ionizer [13-17] or by electron impact ionization [11,12]. The sources described in the present report all utilize surface ionization for the production of cesium ion beams which are used to sputter the sample material. Negative ion sources, based on the sputter principle, thus all share in common the influences of the intrinsic energy and angular distribution characteristics of the sputter process [20] on the emittances of extracted ion beams.

State-of-the-art negative ion sources based on the sputter principle, utilized in the present studies, are described below. The sources differ only in the geometry of the ionizer, its spacing in relation to the negatively biased sample, the spacing of the sample in relation to the ion exit aperture, and the aperture size. The spherical [17], ellipsoidal [8], and cylindrical

geometry [16] sources were designed and developed at the Oak Ridge National Laboratory, while the General Ionex Corporation Model 860 negative source [5] was developed by the University of Pennsylvania [15]. This source is marketed as an integral part of a small tandem accelerator by General Ionex Corporation for use in high-energy ion implantation applications. A source almost identical in design to that of the Model 860 (SNICS II) is used by the National Electrostatics Corporation [4] in similar applications. Because of the similar electrode spacing and construction of this source, the emittance is expected to be very close to that of the Model 860 source.

4.1. The Source Equipped with a Spherical Geometry Ionizer

The source equipped with a spherical geometry ionizer is shown in Fig. 2. The emittance of the source has also been reported previously [9]. The positive cesium ion beam current density distribution at impact with the sample surface is ~ 0.75 mm full diameter whenever the sample is positioned at the focal point of the system. This particular ionizer geometry does not exhibit a halo beam surrounding the high-density distribution. Therefore, the high-density central region of the negatively based sample serves as the sole region from which negative ion beams are generated within the source.

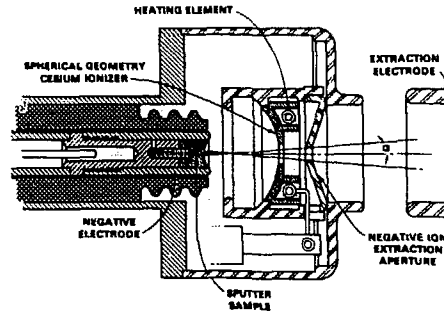

Fig. 2. Schematic drawing of the ion formation and extraction region of the negative ion source equipped with a solid tungsten spherical geometry cesium ionizer.

4.2. The Source Equipped with an Ellipsoidal Geometry Cesium Ionizer

A detailed description of this source (Fig. 3) has not been given previously. However, the emittances and brightnesses of this source have been reported [8]. Computational simulation techniques were utilized in designing the ionizer/sputter probe regions of this source. The observed sample wear pattern which defines the negative ion generation region of the source agrees almost in detail with those computationally predicted. For standard geometry operation, the sample is placed at the focal point of the positive cesium ion beam; the positive ion current density distribution on the sample surface determines the region of negative ion generation, which, in conjunction with the aperture size, the aperture position from the sample surface, and characteristics of the sputter process, essentially determines the emittance of extracted ion beams.

The size and shape of the observed wear patterns for these sources, as well as those computationally predicted, are very sensitive to sample position because of the strongly convergent nature of the extracted cesium ion beam. The wear pattern at the focal point of the electrode system has a diameter of

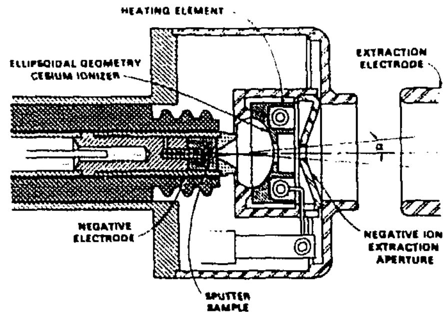

Fig. 3. Schematic drawing of the ion formation and extraction region of the negative ion source equipped with a solid tungsten ellipsoidal geometry cesium ionizer.

Ø ≅ 1.25 mm. The source is routinely placed at the focal position during normal source operation. This source configuration, as well as that of the spherical geometry source just described, does not exhibit a halo beam surrounding the central high-density region.

4.3. The Source Equipped with a Cylindrical Geometry Ionizer

The cylindrical geometry ionizer source configuration is shown in Fig. 4. The computed cesium ion current density distribution and observed sample wear patterns agree remarkably well. The observed wear pattern from this source is composed of two parts: a region of concentrated wear with full diameter of ~ 0.75 mm, and a low-density, uniform-wear region with a diameter of ~ 4.5 mm. Thus, the negative ion beam extracted from the source is composed of beams of two distinctly different characters: (1) a very small source located on axis, and (2) a uniformly distributed halo beam surrounding the central high-density region. Thus, both beams are expected to contribute to the emittance and perhaps increase its value over the previously described sources equipped with spherical and ellipsoidal geometry ionizers.

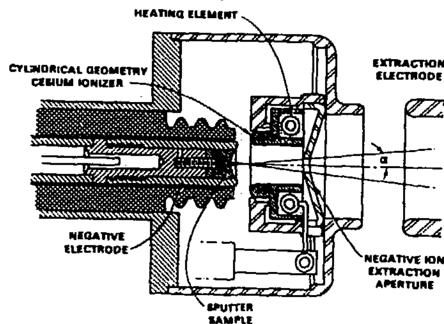

Fig. 4. Schematic drawing of the ion formation and extraction region of the negative ion source equipped with a solid tungsten cylindrical geometry cesium ionizer.

4.4. The Source Equipped with a Spiral-Wound Tantalum Ionizer (General Ionex Corporation Model 860 Negative Ion Source)

The sample wear patterns from the Model 860 source (Fig. 5) were found to be considerably more complex than those of the other sources. Typically, the central region of the sample was found to be strongly worn with a wear diameter of $\emptyset \approx 1$ mm surrounded by a large-diameter ($\emptyset \approx 8$ mm) asymmetrically worn halo beam. The asymmetrical wear pattern within the halo region is attributable to the spiral character of the tantalum ionizer. The presence of the rather large halo beam, as was the case with the source equipped with a cylindrical geometry, will, no doubt, contribute appreciably to the emittance of the source.

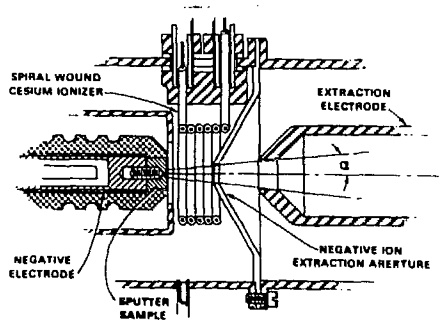

Fig. 5. Schematic drawing of the ion formation and extraction region of the Model 860 negative ion source.

4.5. Negative Ion Source Geometrical Data

Table 1 lists the spatial positions of sputter samples in relation to the ion extraction aperture, aperture size, and emittance estimates based on simple geometric arguments for the Oak Ridge sources with continuous tungsten spherical, ellipsoidal, and cylindrical geometry cesium ionizers and two commercially available sources equipped with spiral-wound tantalum ionizers.

4.6. Negative Ion Source Intensity Data

The negative ion beam intensities which can be extracted from the sources previously described depend on a number of factors. According to the surface ionization model, the efficiency of negative ion formation depends on the electron efficiency E_A of the species in question, the intrinsic work function $\emptyset_o$ of the material from which it was sputter ejected, and the electron affinity E_A and first ionization potential I of the adsorbate utilized to enhance negative ion formation and the adsorbate surface coverage [18,19]. In the sources described in this report, the adsorbate most often utilized is cesium. The rate of negative ion generation depends on the magnitude of the cesium ion current used to sputter the sample material, which, in turn, depends on the source operational parameters, e.g., the cesium oven temperature and sputter probe voltage. The space charge limited cesium current I^+ which can be accelerated at a given sputter probe voltage V and subsequently used for sputtering the sample depends on the perveance k of the electrode configuration according to

$$I^+ = k\, V^{3/2}.$$

Table 1. Estimated Emittances of Negative Ion Sources Equipped with Spherical, Ellipsoidal, Cylindrical Tungsten, and Spiral-Wound Tantalum Cesium Surface Ionizers. Energy: 20 keV.

Source	Sample Distance to Aperture	Ion Exit Aperture Diameter	Assumed Sample Wear Pattern Diameter	Ion Emission Half Angle	Estimated Emittance
	l (mm)	Ø (mm)	s (mm)	α(mrad)	ε(πmm mrad (MeV)$^{1/2}$)
Spherical geometry tungsten	33.3	4.76	1.0	86	6.1
Ellipsoidal geometry tungsten	29.7	4.76	1.25	101	9.0
Cylindrical geometry tungsten	23.0	4.76	1.0	124	8.7
Spiral-wound tantalum (Model 860)	14.3	6.36	1.0	257	17.8
Spiral-wound tantalum (SNICS II)	15.88	6.36	1.0	232	16.4

The negative ion current which can be extracted from the total current generated in the sputter process depends on the size of the negative ion generation region on the sample surface, the angular distribution of the negative ion current at the ion extraction aperture, the spacing of the sample in relation to the aperture, and the aperture size. Because of operational variables and the differences in the ionizer/sample electrode configuration, the negative ion currents will, in general, differ from source to source, and for a particular source vary from operational period to operational period. Negative ion yields for a particular species will depend on the chemical composition of the sample, as well. Table 2 presents the ranges of maximum negative ion intensities which have been realized by a number of investigators through the use of the sources described in this report.

5. Emittance and Brightness Determinations

The previously described equipment and procedures were used in determining the emittances of dc ion beams extracted from sources equipped with spherical, ellipsoidal, and cylindrical solid tungsten cesium surface ionizers and from the Model 860 negative ion source. Emittance measurements were made for negative ion beams of a variety of species ($^{12}C^-$, $^{28}Si^-$, $^{58}Ni^-$, $^{107}Ag^-$, and $^{197}Au^-$) over a range of ion beam intensities ($4 < I < 60$ μA). During these measurements, a search was made for such effects as the dependence of emittance on ion beam intensity, mass, and species. Due to the large amount of data accumulated, it will not be possible to show all of the results of these studies. Therefore, only a selected number of examples will be presented in this report.

Table 2. A Partial List of Negative Ion Currents Observed from High-Intensity Negative Ion Sources Based on the Cesium Sputter Principle.

Ion Species	Cathode Material	Current (μA)
$^{1}H^{-}$	Titanium hydride, Vanadium hydride	10 → 200
$^{10}B^{-}$	Enriched ^{10}B and Al powder, sintered	2 → 60
$^{10}B_2^{-}$	Enriched ^{10}B and Al powder, sintered	4 → 80
$^{12}C^{-}$	High-density graphite	100 → 250
$^{16}O^{-}$	Metal oxides	150 → 500
$^{27}Al^{-}$	Aluminum metal	1 → 4
$^{28}Si^{-}$	Silicon crystal	50 → 800
$^{32}S^{-}$	Metal sulfides	50 → 200
$^{32}P^{-}$	Metal phosphides	10 → 120
$^{63}Cu^{-}$	Copper metal	50 → 150
$^{75}As^{-}$	Gallium arsenide and Al powder	10 → 80
$^{58}Ni^{-}$	Nickel metal	10 → 150
$^{80}Se^{-}$	Cadmium sellenide	20 → 100
$^{194}Pt^{-}$	Platinum metal	25 → 66
$^{197}Au^{-}$	Gold metal	50 → 200

5.1. Emittance Data

5.1.1. Spherical Geometry Ionizer Source. The results derived from measurements of the emittances versus percentage total negative ion current extracted from an Ag sample in the spherical geometry ionizer source for total beam currents of 4, 6, 8, 10, and 12 μA are displayed in Fig. 6. Over the range of negative ion currents investigated, there is no evidence of the rather strong dependence of emittance on negative ion current as found by Doucas, Hyder, and Knox [21] for ion beams extracted from the cone geometry negative sputter ion source. Such increases are most probably attributable to changes in emission area due to changes in the positive ion beam size at impact induced by positive ion beam space charge effects.

5.1.2. The Ellipsoidal Geometry Ionizer Source. Emittance versus percentage negative ion beam intensity data for various negative ion beams of $^{12}C^{-}$ extracted from the ellipsoidal geometry ionizer source are displayed in Fig. 7. These data suggest a moderate increase in the emittance for the 80% contour level with increasing ion beam intensity of perhaps 20% over an intensity range of $20 < I < 50$ μA. These findings are also in contrast to the rather large increases in emittance with ion beam intensity found by Doucas,

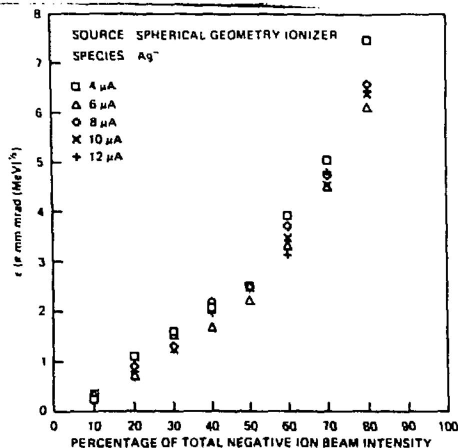

Fig. 6. Emittance, ε, versus percentage of negative ion beam for various negative ion beam intensities of Ag^- extracted from the source equipped with a spherical geometry ionizer.

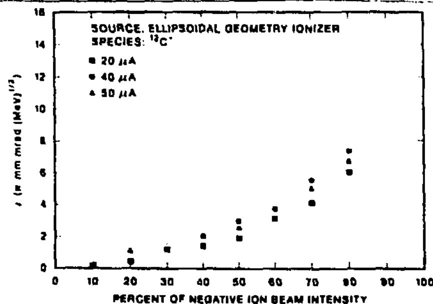

Fig. 7. Emittance, ε, versus percentage of negative ion beam for various negative ion beam intensities of $^{12}C^-$ extracted from the source equipped with an ellipsoidal geometry ionizer.

Hyder, and Knox [21] for ion beams extracted from the cone geometry negative ion source. However, for other data sets not shown, the effect, if it exists, is obscured by statistical fluctuations. No evidence of a monotonic dependence of emittance on ion mass was found. These findings, thus, support those made earlier by Doucas, Hyder, and Knox.

5.1.3. Cylindrical Geometry Ionizer Source. Emittance data for $^{28}Si^-$ ion beams extracted from the source equipped with a cylindrical geometry cesium ionizer are displayed in Fig. 8. These data also show the presence of a moderate increase in emittance with increasing ion beam intensity over the range of intensities investigated. For example, the effect is seen to be ~ 9% for $^{28}Si^-$ at the 80% contour level over an intensity range of $16 < I < 20$ μA. Similar increases were also noted for $^{12}C^-$, $^{58}Ni^-$, and $^{197}Au^-$ data (not shown) over an intensity range $5 < I < 60$ μA. However, the increases observed in the above data may, in fact, be attributable to changes in the size of the cesium beam at impact with acceleration voltage V, in which case, the overall effect would be independent of negative ion species, but would change with cesium ion energy.

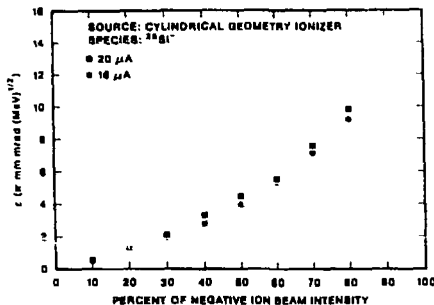

Fig. 8. Emittance, ε, versus percentage negative ion beam for various beam intensities of $^{28}Si^-$ extracted from the source equipped with a cylindrical geometry cesium ionizer.

5.1.4. The Model 860 Source. Emittance data similar to those shown previously for the ellipsoidal and cylindrical geometry ionizer sources are displayed in Fig. 9 for $^{58}Ni^-$ ion beams extracted from the Model 860 source. These data, as well as data for $^{12}C^-$, $^{28}Si^-$, and $^{197}Au^-$ (not shown), exhibit no evidence of significant intensity, species, or mass dependence.

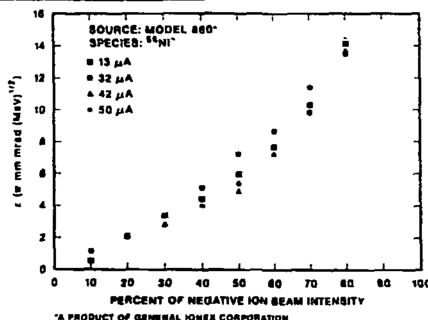

Fig. 9. Emittance, ε, versus percentage negative ion beam for various beam intensities of $^{58}Ni^-$ extracted from the Model 860 ion source.

5.2. Comparative Average Emittance and Brightness Data

If we ignore the presence of intensity, species, or mass-dependent effects and perform an average of all emittance contour data, we obtain the average emittance versus percentage negative ion beam intensity data shown in Fig. 10. The emittance for a given contour of a beam extracted from the Model 860 source is observed to be considerably higher than those for the same contour associated with beams extracted from the spherical, ellipsoidal, and cylindrical ionizer geometry negative ion sources.

Fig. 11 displays average brightness B versus percentage average negative ion beam intensity for the four subject sources. The average emittance data (discussed above) was used in conjunction with the average ion beam intensity to compute the brightness B.

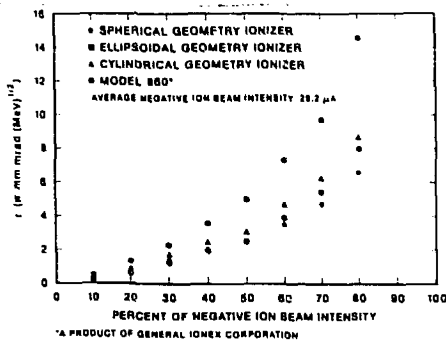

Fig. 10. Average emittance, ε, versus percentage average negative ion beam intensity for beams extracted from sources equipped with spherical, ellipsoidal, and cylindrical geometry cesium ionizers and the Model 860 negative ion source.

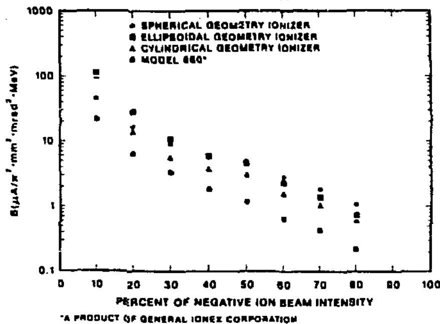

Fig. 11. Average brightness, B, versus percentage average negative ion beam for beams extracted from sources equipped with spherical, ellipsoidal, and cylindrical geometry cesium ionizers and the Model 860 negative ion source.

5.3. Source Compatibility with Accelerator Acceptance

In order to determine the compatibility of a particular ion implantation system, the acceptance A of the accelerator must be known or calculable. For small tandem accelerators suitable for use in ion implantation applications, the gas stripping canal acts as the limiting element in the accelerator; the acceptance A of the accelerator then may be approximated by the acceptance of the stripper and of length L bounded by two apertures of full diameters $\emptyset_1 = 2r_1$ and $\emptyset_2 = 2r_2$ is given by [22]

$$A = \frac{\pi r_1 r_2}{L}.$$

The normalized acceptance for the General Ionex Corporation 1.7-MV Tandetron accelerator [5] (r_1 = 3.5 mm, r_2 = 3.5 mm, L = 711 mm) is

$$A_n = 23.2\ \pi.\text{mm.mrad(MeV)}^{1/2},$$

while the acceptance of the 3-MV tandem accelerator marketed by the National Electrostatics Corporation [4] (r_1 = 5 mm, r_2 = 5 mm, L = 660 mm) is

$$A_n = 65.6\ \pi.\text{mm.mrad(MeV)}^{1/2}.$$

Thus, the acceptance of these two commercially available, high-energy, ion implantation accelerators are each large with respect to the emittances of all of the sources described in this report. Of course, some allowance should be made for multiple scattering degradation of the ion beam emittances during the stripping process.

6. Summary and Conclusions

The emittances for the 80% contour level of the Model 860 source are factors of 2.4, 1.8, and 1.7 higher, respectively, than those for the same contour from sources equipped with spherical, ellipsoidal, and cylindrical geometry cesium ionizers. These average data are representative and typical of all values derived from measurements associated with a particular ion species and ion beam intensity.

It is interesting to note that the emittance values for the 80% contours for the four sources agree closely with the estimations based on simple geometrical arguments made in Table 1; i.e., the product of the full width of the high-density portion of the cesium ion beam at impact with the probe surface and the angular divergence limitation imposed by the exit aperture of the particular ion source.

At the 10% contour level the spherical geometry source has a brightness of ~ 2.2 times, and at the 80% level, an average brightness of 4.9 times that of the Model 860 source, while the ellipsoidal geometry source has an average brightness of ~ 5.4 times at the 10% level, and at the 80% level, an average brightness of ~ 3.5 times that of the Model 860 source. On the other hand, the cylindrical geometry ionizer source has a brightness at the 10% contour level of ~ 4.3 times and at the 80% level ~ 3 times that of the Model 860 source.

All sources evaluated have emittances compatible with commercially available tandem accelerators suitable for use in high-energy ion implantation applications.

7. Acknowledgements

The author is indebted to Ms. Jeanette McBride for skillful typing of the manuscript and to the National Electrostatics Corporation, Middleton, Wisconsin, for supplying useful information concerning the yields from the SNICS II negative ion source.

8. References

1. W. R. Fahrner, J. R. Laschinski, and D. Brunig, Proceedings of the Seventh Tandem Conference, Berlin, W. Germany, April 6-10, 1987, to be published in Nucl. Instrum. and Meth. in Phys. Res.

2. Proceedings of the Fifth Conference on Ion Implantation, Smuggler's Notch, Vermont, July 1984, eds. J. F. Ziegler and R. L. Brown.

3. H. F. Glavish, Nucl. Instrum. and Meth. in Phys. Res. B24/25 (1987) 771.

4. National Electrostatics Corporation, Middleton, WI.

5. General Ionex Corporation, Newburyport, MA.

6. N. R. White, General Ionex Corporation, Newburyport, MA, private communication.

7. T. R. Walsh, J. Nucl. Energy, Pt.C. 4 (1962) 53; T. R. Walsh, J. Nucl. Energy, Pt.C. 5 (1963) 17.

8. G. D. Alton and J. W. McConnell, Proceedings of Seventh Tandem Conference, Berlin, W. Germany, April 6-10, 1987, to be published in Nucl. Instrum. and Meth. in Phys. Res.

9. G. D. Alton, J. W. McConnell, S. Tajima, and G. J. Nelson, Nucl. Instrum. and Meth. in Phys. Res., B24/25 (1987) 826.

10. V. E. Krohn, Jr., Appl. Phys. 33 (1962) 3523.

11. H. H. Andersen and P. Tykesson, IEEE Trans. Nucl. Sci. NS-22 (1975) 1632; P. Tykesson, H. H. Anderson, and J. Heinemeier, IEEE Trans. Nucl. Sci., NS-23, No. 2 (1976) 1104.

12. G. D. Alton and G. C. Blazey, Nucl. Instr. and Meth. 166 (1979) 105; G. D. Alton, R. M. Beckers, and J. W. Johnson, ibid, 148.

13. G. T. Caskey, R. A. Douglas, H. T. Richards, and H. V. Smith, Jr., Nucl. Instr. and Meth. 157 (1978) 1.

14. G. D. Alton, IEEE Trans. Nucl. Sci. NS-26 (3) (1979) 3708.

15. R. Middleton, Nucl. Instr. and Meth. 214 (1983) 139.

16. G. D. Alton, Nucl. Instr. and Meth. A244 (1986) 133.

17. G. D. Alton and G. D. Mills, IEEE Trans. Nucl. Sci. NS-32 (5) (1985) 1822.

18. G. D. Alton, Surf. Sci. 175 (1986) 226.

19. J. K. Nørskov and B. I. Lundquist, Phys. Rev. B 19, 5661 (1979).

20. R. Behrisch, ed. 1981, Sputtering by Particle Bombardment, Vol. 47 (New York: Springer).

21. G. Doucas and H. R. Mck. Hyder, Nucl. Instr. and Meth. 119 (1974) 413; G. Doucas, H. R. Mck. Hyder, and A. B. Knox, Nucl. Instr. and Meth. 124 (1975) 11.

22. J. D. Larson and C. M. Jones, Nucl. Instrum. and Meth. 140 (1977) 489.